2-D Circuit-based Bianisotropic Omega Media

Luke Szymanski, Student, IEEE, Anthony Grbic, Fellow, IEEE

Abstract—In one dimension, a circuit network representation has been established for bianisotropic materials with an omega response (omega media). However, 2-D circuit-based or transmission-line metamaterials have been restricted to those with only magnetic and electric responses. This paper proposes a 2-D circuit-based metamaterial that is equivalent to an omega medium. A lumped element unit cell composed of asymmetric π -networks is proposed and validated using a circuit simulator. A circuit analysis of the metamaterial is performed using transmission (ABCD) matrices. A medium equivalency is then established in the homogeneous limit. The application of a 2-D omega medium as an impedance matching layer with phase and power flow control is explored and a design procedure is developed. The impedance matching layer is then implemented using the proposed lumped element unit cell, and its performance is confirmed using Keysight's Advanced Design System (ADS).

Index Terms—bianisotropic media, periodic structures, electromagnetic propagation, circuit modeling

I. INTRODUCTION

PERIODIC circuit networks have been used to model electromagnetic wave propagation in continuous media since Heaviside introduced the transmission line model in the late 19th century. The transmission line model uses a two-port, lumped element unit cell to represent an infinitesimal transmission line section. Performing circuit analysis on the unit cell and taking the infinitesimal limit results in the well known Telegrapher's equations. In this way a link between wave propagation on a transmission line and propagation in a periodic circuit network is established. Further, the connection between transverse electromagnetic (TEM) waves in an unbounded medium and a TEM mode on a transmission line links unguided waves in continuous media to guided waves on circuit networks.

These links provided by the transmission line model inspired artificial transmission lines used in telephonic transmission applications [1]. The model has also been used in numerical electromagnetics forming the basis of the transmission line matrix (TLM) method, [5]. In the early 2000's the introduction of 1-D circuit-based or transmission-line (TL) metamaterials renewed interest in circuit analogies of electromagnetic media [2], [3]. This work allowed for the synthesis of a wide range of effective material properties including a negative index. This enabled several of the phenomena predicted by Veselago, [4], to be observed [3], [7]. Following the introduction of 1-D TL metamaterials, isotropic 2-D TL metamaterials followed [12], allowing for the verification of sub-diffraction imaging

Manuscript received September 17, 2019; revised March 27, 2020; accepted May 11, 2020. This work was supported by the NSF under GOALI grant (1807940)

The authors are with the Radiation Laboratory, Department of Electrical Engineering and Computer Science, University of Michigan, Ann Arbor MI 48109-2122 USA (email: agrbic@umich.edu).

using a negative index lens, [13]. Subsequently, it was demonstrated that TL metamaterials can provide anisotropic [14] and tensor material responses, aiding in the realization of a wide range of transformation optics designs [17]–[19]. In [20], 1-D bianisotropic metamaterials with an omega response were introduced using asymmetric 1-D circuit networks. However, a circuit-based equivalent to 2-D bianisotropic metamaterials possessing an omega response has not been reported to date.

Lossless bianisotropic media with an omega response (omega media) have complex wave impedances, making them well suited for impedance matching. This property has been exploited in bianisotropic metasurfaces that perform reflectionless field transformations, [21]–[24], and wideband impedance matching [25]. These metasurfaces locally conserve the normal power density across their surface, i.e. in a pointwise manner, limiting these metasurfaces to control over transmission phase. Amplitude control can be achieved using a pair of metasurfaces with an electrically large spacing between them to reshape the power density profile, [26]-[28]. However, these designs require conservation of normal power density across each constitutive metasurface and are electrically large. Another method to achieve discontinuities in normal power density is to convert a propagating wave to a surface wave. This can be achieved with either a reflective metasurface that couples to a surface wave in the same region as the incident wave [29], or a bianiostropic metasurface that locally conserves normal power denisty and couples to a surface wave in the transmitted region [30].

Typically, omega-type metasurfaces are realized with cascaded impedance sheets [21], [31]. Local conservation of normal power density (neglecting transverse coupling) necessitates extremely sub-wavelength spacings between the sheets or metallic walls to isolate neighboring unit cells. However, if transverse coupling is accounted for in the design of metasurfaces, the incident and transmitted power density profiles could be made different. Metasurfaces that utilize transverse coupling could offer greater design freedom and eliminate the need to isolate neighboring unit cells.

In [32], it was established that tangential polarizabilities are sufficient to establish any transmission phase without reflection. However, designs with only tangential polarizabilities can exhibit significantly degraded performance when compared to equivalent realizations utilizing normal polarizabilities. Previously, it was shown that a material with tangential and normal polarizabilities (an inhomogeneous 2-D anisotropic medium) can control phase and power flow to perform field transformations [33]. However, these devices were electrically large because impedance matching and controlling transmission phase is not possible with an anisotropic medium. The complex wave impedance of 2-D omega media could be used to reduce the size of the these devices, providing a route

1

to design electrically thin layers that do not require local conservation of normal power density.

There are two major challenges associated with designing a 2-D omega metamaterial: (a) synthesis of the necessary 2-D omega material parameters and (b) simulating the omega material design. This work aims to address these issues through the development of a circuit-based model for omega media. A circuit model will allow for the materials to be fabricated as 2-D transmission line networks and simulated using commercial circuit solvers. The circuit model is analyzed as a general 2-D periodic circuit network composed of 1-D asymmetric circuit networks. The dispersion relation and wave impedance are then taken in the homogeneous limit to establish an equivalence with a 2-D reciprocal and lossless omega medium. This circuit equivalent is then used to design a 2-D omega slab that acts as an impedance matching layer. The impedance matching layer provides a desired phase delay and translates the power density profile of the incident wavefront.

II. 1-D BIANISOTROPIC OMEGA MATERIALS

The constitutive relations for a bianisotropic medium are,

$$\overline{D} = \overline{\overline{\varepsilon}} \cdot \overline{E} + \overline{\overline{a}} \cdot \overline{H} \tag{1}$$

$$\overline{B} = \overline{\overline{\mu}} \cdot \overline{H} + \overline{\overline{b}} \cdot \overline{E} \tag{2}$$

If the medium has an omega response, the magneto-electric dyadics are anti-symmetric: $\overline{\overline{a}}=-\overline{\overline{a}}^T$ and $\overline{\overline{b}}=-\overline{\overline{b}}^T$. Further, if it is lossless $\overline{\overline{\varepsilon}}$ and $\overline{\overline{\mu}}$ are purely real and $\overline{\overline{a}}$ and $\overline{\overline{b}}$ are purely imaginary. Additionally, reciprocity requires $\overline{\overline{\varepsilon}}=\overline{\overline{\varepsilon}}^T$, $\overline{\overline{\mu}}=\overline{\overline{\mu}}^T$, and $\overline{\overline{b}}=-\overline{\overline{a}}^T$.

In [20], the equivalence between TEM propagation along a lossless, reciprocal, omega medium and propagation in a 1-D periodic circuit network was established. The dispersion relation and wave impedance for a lossless and reciprocal 1-D omega medium are,

$$k^{\pm 2} = \omega^2 (\mu \varepsilon + a^2) \tag{3}$$

$$\eta^{\pm} = \frac{\omega \mu}{k^{\pm} - \omega a} \tag{4}$$

where the permeability, μ , and permittivity, ε , are purely real, the magneto-electric coupling, a, is purely imaginary, and the wavenumber is $k^{\pm} = \pm k^{'} - jk^{''}$. The \pm superscripts are included to differentiate between forward and reverse propagating waves.

Performing Bloch analysis on a periodic network with period d, composed of a lossless and reciprocal electrical network represented by a transmission (ABCD) matrix (see Fig. 1), yields the following dispersion relation and Bloch impedance

$$\sin^2 k_B^{\pm} d = -BC + \left(j \frac{D - A}{2}\right)^2 \tag{5}$$

$$Z_B^{\pm} = \frac{-jB}{\sin k_B^{\pm} d - j\frac{D-A}{2}} \tag{6}$$

where the Bloch wavenumber $k_B^{\pm}=\pm k_B^{'}-jk_B^{''}$, [37]. Since the network is lossless, A and D are purely real while B and C are purely imaginary. Further, reciprocity requires that

$$AD - BC = 1. (7)$$

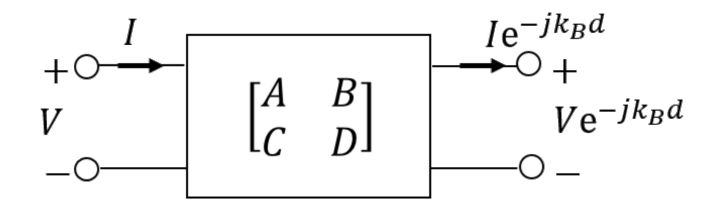


Fig. 1. Transmission (ABCD) matrix representing a unit cell of a one-dimensional periodic circuit network.

In the homogeneous limit, $|k_B^{\pm}d| \ll 1$, so (5) and (6) become,

$$(k_B^{\pm}d)^2 = -BC + \left(j\frac{D-A}{2}\right)^2 \tag{8}$$

$$Z_B^{\pm} = \frac{-jB}{k_B^{\pm}d - j\frac{D-A}{2}} \tag{9}$$

Comparing (3) with (8), and (5) with (9), reveals the following equivalency between the asymmetric network $(A \neq D)$ and an omega medium,

$$\mu = -j\frac{B}{\omega d}, \quad \varepsilon = -j\frac{C}{\omega d}, \quad a = j\frac{D - A}{2\omega d}$$
 (10)

It should be noted that although these expressions are different from those presented in [20], they are equivalent.

III. 2-D BIANISOTROPIC OMEGA MATERIALS

A. Field Theory

There are two major classes of reciprocal bianisotropic media: chiral and omega. This work focuses on TE polarized plane waves in a lossless bianisotropic omega-type medium, i.e. a reciprocal bianisotroic medium with an omega response. To maintain a TE polarization it is assumed that the medium preserves polarization. That is, induced magnetic flux densities are along the same axes as the magnetic field and the induced electric flux densities are along the same axes as the electric field. For a TE plane wave propagating in the x-z plane, its wavevector is $\overline{k} = k_x \hat{x} + k_z \hat{z}$, and the relevant fields are, $\overline{E} = E \hat{y}$ and $\overline{H} = H_x \hat{x} + H_z \hat{z}$. The permittivity, $\overline{\varepsilon}$, has one relevant entry, ε_{yy} , and the remaining relevant material parameters are,

$$\overline{\overline{\mu}} = \begin{bmatrix} \mu_{xx} & 0\\ 0 & \mu_{zz} \end{bmatrix} \tag{11}$$

$$\overline{\overline{a}} = \overline{\overline{b}} = \begin{bmatrix} 0 & -ja_{xy} & 0\\ ja_{xy} & 0 & ja_{zy}\\ 0 & -ja_{zy} & 0 \end{bmatrix}$$
(12)

For an $e^{j\omega t}$ time convention and TE plane wave propagation in the x-z plane, Faraday and Ampere's laws can be written as the following system of equations,

$$-k_z \frac{E_y}{H_x} = \omega(\mu_{xx} - ja_{xy} \frac{E_y}{H_x}) \tag{13}$$

$$k_x \frac{E_y}{H_z} = \omega (\mu_{zz} - ja_{zy} \frac{E_y}{H_z}) \tag{14}$$

$$k_z \frac{H_x}{E_y} - k_x \frac{H_z}{E_y} = -\omega(\varepsilon_{yy} + ja_{xy} \frac{H_x}{E_y} + ja_{zy} \frac{H_z}{E_y})$$
 (15)

Solving (13)–(15), the dispersion relation and wave impedances along the principal axes of the medium can be written,

$$\frac{k_x^{\pm 2} + (\omega a_{zy})^2}{\omega \mu_{zz}} + \frac{k_z^{\pm 2} + (\omega a_{xy})^2}{\omega \mu_{xx}} = \omega \varepsilon_{yy}$$
 (16)

$$\eta_x^{\pm} = \frac{E_y}{H_z} = \frac{\omega \mu_{zz}}{k_x^{\pm} + j\omega a_{zy}} \tag{17}$$

$$\eta_z^{\pm} = -\frac{E_y}{H_x} = \frac{\omega \mu_{xx}}{k_z^{\pm} - j\omega a_{xy}} \tag{18}$$

where $k_x^{\pm}=\pm k_x^{'}-jk_x^{''}$ and $k_z^{\pm}=\pm k_z^{'}-jk_z^{''}$. The \pm superscripts differentiate between the forward and reverse propagating fields.

B. Circuit Theory

For comparison with a 2-D omega medium, a 2-D periodic circuit network with the unit cell depicted in Fig. 2 will be analyzed. It is composed of four branches of 1-D constituent circuit networks. The two constituent networks along a single direction (x or z) are the same. It is important to note that if the constituent networks are asymmetric the overall unit cell is asymmetric. The propagation characteristics of this network can be determined using the analysis procedure presented in [8]. The dispersion relation and Bloch impedances for the network in Fig. 2 are,

$$\frac{\sin^2 \frac{k_{Bx}^{\pm}d}{2} + \left(\frac{A_1 - D_1}{2}\right)^2}{jB_1\left(\frac{jC_1}{A_1 + D_1} + \frac{jC_2}{A_2 + D_2}\right)(A_1 + D_1)} + \frac{\sin^2 \frac{k_{Bz}^{\pm}d}{2} + \left(\frac{D_2 - A_2}{2}\right)^2}{jB_2\left(\frac{jC_1}{A_1 + D_1} + \frac{jC_2}{A_2 + D_2}\right)(A_2 + D_2)} = 1 \quad (19)$$

$$Z_{Bx}^{\pm} = \frac{-j\frac{2B_1}{A_1 + D_1}}{\tan\frac{k_{Bx}^{\pm}d}{2} + j\left(\frac{A_1 - D_1}{A_1 + D_1}\right)} \tag{20}$$

$$Z_{Bz}^{\pm} = \frac{-j\frac{2B_2}{A_2 + D_2}}{\tan\frac{k_{Bz}^{\pm}d}{2} - j(\frac{D_2 - A_2}{A_2 + D_2})}$$
(21)

where, $k_{Bx}^{\pm}=\pm k_{Bx}^{'}-jk_{Bx}^{''}$ and $k_{Bz}^{\pm}=\pm k_{Bz}^{'}-jk_{Bz}^{''}$, and $A_{1,2},\,B_{1,2},\,C_{1,2},$ and $D_{1,2}$ satisfy the lossless and reciprocal conditions for an ABCD matrix given by (7). Two constraints are imposed on electrical lengths within the circuit network. One constraint is on the electrical lengths of the constituent networks and the second is on the electrical lengths of the overall unit cell which, are not necessarily equivalent conditions. The first constraint reduces spatial dispersion within the unit cell, while the second constraint allows for homogenization of the unit cell. The first constraint can be satisfied by observing from 1-D periodic analysis that the electrical length, $k_{B_{1,2}}\frac{d}{2}$, of each constitutive network is given by $\cos(k_{B_{1,2}}\frac{d}{2})=(A_{1,2}+D_{1,2})/2$. Therefore, requiring the circuit networks to be electrically small is equivalent to mandating that $A_{1,2}+D_{1,2}\approx 2$, since $\cos(x)\approx 1$ as $x\to 0$. Taking the homogeneous limit, i.e. $(k_{Bx,z}^{''}d,k_{Bx,z}^{''}d,\ll 1)$,

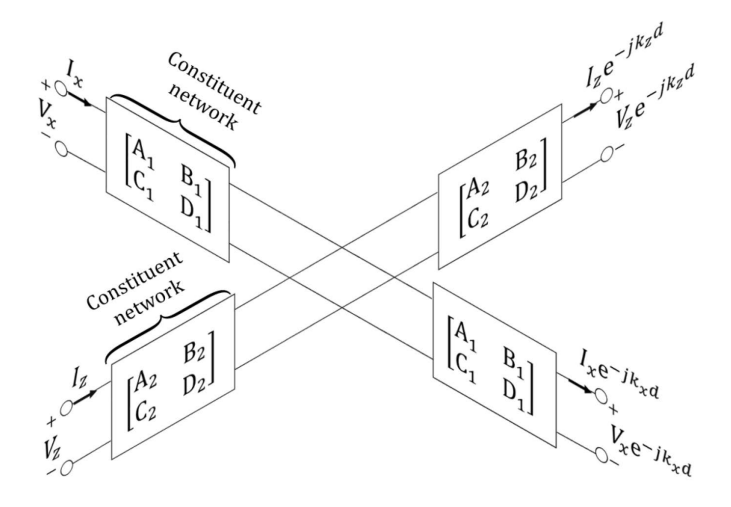


Fig. 2. ABCD matrix representation of a two-dimensional periodic circuit network with common constituent networks along each axis.

assuming the constituent networks are electrically small, and $C_1 + C_2 \neq 0$, (19)–(21) become,

$$\frac{(k_{Bx}^{\pm}d)^{2} + (A_{1} - D_{1})^{2}}{j2B_{1}} + \frac{(k_{Bz}^{\pm}d)^{2} + (D_{2} - A_{2})^{2}}{j2B_{2}} = j2(C_{1} + C_{2}) \quad (22)$$

$$Z_{Bx}^{\pm} = \frac{-j2B_1}{k_{Bx}^{\pm}d + j(A_1 - D_1)}$$
 (23)

$$Z_{Bz}^{\pm} = \frac{-j2B_2}{k_{Bz}^{\pm}d - j(D_2 - A_2)}$$
 (24)

Comparing these expressions to those from field theory reveals a one-to-one relationship between (16)–(18) and (22)–(24). Therefore, if the 1-D constitutive networks are electrically small, and the unit cell can be homogenized, the 2-D network shown in Fig. 2 behaves like an omega medium with material parameters,

$$\mu_{xx} = -j\frac{2B_2}{\omega d}, \quad \mu_{zz} = -j\frac{2B_1}{\omega d}, \quad \varepsilon_{yy} = -j\frac{2(C_1 + C_2)}{\omega d}$$

$$a_{xy} = \frac{D_2 - A_2}{\omega d}, \quad a_{zy} = \frac{A_1 - D_1}{\omega d}$$
(25)

For a simpler comparison between the 1-D and 2-D effective material parameters, consider the situation where the ABCD parameters in all of the constitutive networks are halved, then (25) becomes,

$$\mu_{xx} = -j\frac{B_2}{\omega d}, \quad \mu_{zz} = -j\frac{B_1}{\omega d}, \quad \varepsilon_{yy} = -j\frac{(C_1 + C_2)}{\omega d}$$

$$a_{xy} = \frac{D_2 - A_2}{2\omega d}, \quad a_{zy} = \frac{A_1 - D_1}{2\omega d}$$
 (26)

Comparing (26) to (10) reveals that the relationship between a 1-D circuit network's ABCD-parameters and its effective material parameters is the same as a 2-D network's with the exception of the permittivity. The effective permittivity is the sum of the permittivities of the constituent networks, as previously observed in isotropic transmission-line grids [2].

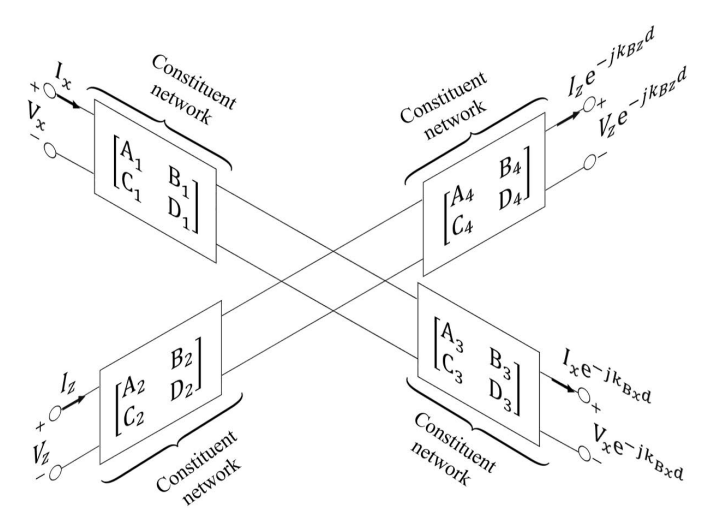


Fig. 3. ABCD matrix representation of a generalized two-dimensional periodic circuit network where all constituent networks are different.

A notable feature of both (10) and (25) is that the magneto-electric response is proportional to the difference between A and D. Therefore, if there is no asymmetry in the constituent networks the magneto-electric response disappears. This is consistent with the fact that asymmetry gives rise to magneto-electric effects in omega-type bianisotropic media, [20], [35].

C. Asymmetry in 2-D Periodic Circuit Networks

As previously noted, bianisotropic responses arise in periodic circuit networks if their unit cells are asymmetric. In this section, different types of asymmetries and their effects on the general 2-D unit cell composed of four constituent networks, shown in Fig. 3, will be studied. The unit cell is asymmetric in the x-direction if: (a) $B_1 \neq B_3$ or (b) $D_1 \neq A_3$. Due to reciprocity, the condition $C_1 \neq C_3$ is not a sufficient condition to make the unit cell asymmetric if neither (a) or (b) is satisfied. Similar conditions hold for the z-direction. To gain understanding on the effects of these asymmetries, the periodic network's dispersion relation and Bloch impedances will be studied for different conditions placed on the networks ABCD parameters. The dispersion relation and Bloch impedances for the network shown in Fig. 3 are,

$$\frac{4\sin^2\frac{k_{Bx}^{\pm}d}{2} + \left(\frac{D_1 - A_3}{\sqrt{A_3D_1}}\right)^2}{j(B_1A_3 + B_3D_1)} + \frac{4\sin^2\frac{k_{Bx}^{\pm}d}{2} + \left(\frac{A_4 - D_2}{\sqrt{A_4D_2}}\right)^2}{j(B_2A_4 + B_4D_2)} \\
= j\frac{A_3C_1 + D_1C_3}{A_3D_1} + j\frac{A_4C_2 + D_2C_4}{A_4D_2} \tag{27}$$

$$Z_{Bx}^{\pm} = \frac{-j\left(\Sigma_{B_{13}} + \left(\frac{\Delta_{B_{13}}}{\sqrt{\Sigma_{B_{13}}}}\right)^{2} \tan^{2} \frac{k_{Bx}^{\pm} d}{2}\right) \frac{\Sigma_{B_{13}}}{B_{3}D_{1} + B_{1}A_{3}}}{2 \tan^{2} \frac{k_{Bx}^{\pm} d}{2} - j\left(\Delta_{13} + \frac{\Delta_{B_{13}}}{\Sigma_{B_{13}}} \Sigma_{13} \tan^{2} \frac{k_{Bx}^{\pm} d}{2}\right) \frac{\Sigma_{B_{13}}}{B_{3}D_{1} + B_{1}A_{3}}}$$
(28)

$$Z_{Bz}^{\pm} = \frac{-j\left(\Sigma_{B_{24}} + \left(\frac{\Delta_{B_{24}}}{\sqrt{\Sigma_{B_{24}}}}\right)^2 \tan^2 \frac{k_{Bz}^{\pm}d}{2}\right) \frac{\Sigma_{B_{24}}}{B_4 D_2 + B_2 A_4}}{2 \tan \frac{k_{Bz}^{\pm}d}{2} - j\left(\Delta_{24} + \frac{\Delta_{B_{24}}}{\Sigma_{B_{24}}} \Sigma_{42} \tan^2 \frac{k_{Bz}^{\pm}d}{2}\right) \frac{\Sigma_{B_{24}}}{B_4 D_2 + B_2 A_4}}$$
(29)

where $\Sigma_{B_{ij}}=B_i+B_j$, $\Delta_{B_{ij}}=B_i-B_j$, $\Delta_{13}=D_1-A_3$, $\Sigma_{13}=D_1+A_3$, $\Delta_{24}=D_2-A_4$, and $\Sigma_{42}=A_4+D_2$. In this generalized form, there is no medium equivalence. However, the effects of the different types of asymmetry can be understood. By comparing (17) to (28) one notices that the asymmetry introduced by setting $B_1\neq B_3$ requires spatially dispersive material parameters if the wave impedance is to match that of an omega medium. This is due to the fact that terms proportional to $k_{Bx}^{\pm}d$, occur in (28) when $B_1\neq B_3$. The same effect occurs in the z-directed wave impedance when $B_2\neq B_4$. To eliminate such spatial dispersion, the following conditions are imposed on the constituent networks: $B_1=B_3$ and $B_2=B_4$. Under these constraints (27)–(29) become,

$$\frac{4\sin^2\frac{k_{Bx}^{\pm}d}{2} - \left(j\frac{D_1 - A_3}{\sqrt{A_3D_1}}\right)^2}{jB_1(A_3 + D_1)} + \frac{4\sin^2\frac{k_{Bz}^{\pm}d}{2} - \left(j\frac{A_4 - D_2}{\sqrt{A_4D_2}}\right)^2}{jB_2(A_4 + D_2)}$$

$$= j\frac{A_3C_1 + D_1C_3}{A_3D_1} + j\frac{A_4C_2 + D_2C_4}{A_4D_2} \tag{30}$$

$$Z_{Bx}^{\pm} = \frac{-j\frac{4B_1}{A_3 + D_1}}{2\tan\frac{k_{Bx}^{\pm}d}{2} - j2\frac{D_1 - A_3}{A_3 + D_1}}$$
(31)

$$Z_{Bz}^{\pm} = \frac{-j\frac{4B_2}{A_4 + D_2}}{2\tan\frac{k_{Bz}^{\pm}d}{2} - j2\frac{D_2 - A_4}{A_4 + D_2}}$$
(32)

If it is further assumed that the constituent networks and the unit cells are electrically small, it can be shown that the unit cell in Fig. 2 is required for a one-to-one relationship to exist between (16)–(18) and (30)–(32). Therefore, to limit spatial dispersion in the periodic network the asymmetric unit cell in Fig. 2 was used rather than that in Fig. 3.

IV. EXAMPLES

A. Characterization of a Lumped Element Unit Cell

The equivalency between omega media and the proposed circuit network in Fig. 2 is verified by comparing the simulated dispersion characteristics of the circuit network with the analogous medium's. Isofrequency contours (the intersection of a constant frequency plane with the surface described by the dispersion relation) are used to compare the analogous medium, (16), and the circuit network at a fixed frequency. In order to simulate the proposed unit cell, Fig. 2, a suitable unit cell is chosen such that the asymmetry of the unit cell can be easily tailored. Lumped element T-networks and π -networks are suitable building blocks (see Fig. 4), since they provide asymmetric responses whenever $Z_1 \neq Z_2$ or $Y_1 \neq Y_2$. This can be seen by examining the ABCD parameters of the π and T-networks shown in Fig. 4,

$$\begin{bmatrix} A_{\pi} & B_{\pi} \\ C_{\pi} & D_{\pi} \end{bmatrix} = \begin{bmatrix} 1 + ZY_2 & Z \\ Y_1 + Y_2 + ZY_1Y_2 & 1 + ZY_1 \end{bmatrix}$$
(33)

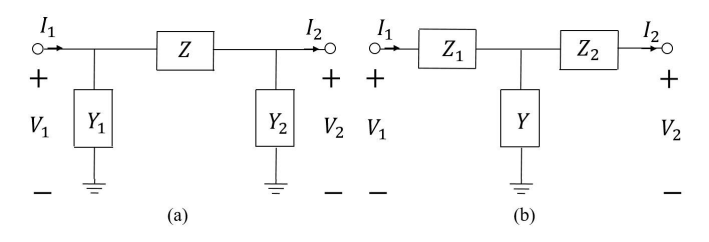


Fig. 4. (a) A lumped element π -network (b) A lumped element T-network.

TABLE I LUMPED ELEMENT VALUES

Element	Value	Element	Value
L_x	3.53 nH	L_z	2.43 nH
C_{x1}	0.58 fF	C_{z1}	0.94 fF
C_{x2}	3 fF	C_{z2}	2.64 fF

The inductor and capacitor values necessary to synthesize a medium with the effective material parameters: $\varepsilon_{yy}=2\varepsilon_0,\ \mu_{xx}=5\mu_0,\ \mu_{zz}=7\mu_0,\ a_{xy}=-a_{yx}=j0.1\sqrt{\mu_0\varepsilon_0},$ and $a_{zy}=-a_{yz}=-j0.2\sqrt{\mu_0\varepsilon_0}$ at a frequency of 10 GHz.

$$\begin{bmatrix} A_T & B_T \\ C_T & D_T \end{bmatrix} = \begin{bmatrix} 1 + Z_1 Y & Z_1 + Z_2 + Z_1 Z_2 Y \\ Y & 1 + Z_2 Y \end{bmatrix}$$
(34)

In both cases, if $Z_1 \neq Z_2$ or $Y_1 \neq Y_2$ then $A \neq D$ and the network is asymmetric. The π -network will be examined because it results in the simplest overall unit cell. To construct the 2-D network, shown in Fig. 2, each constituent network is an asymmetric π -network resulting in the unit cell shown in Fig. 5. It can be further simplified by combining all the shunt elements at the central node, as shown in Fig. 6.

Since C_1 and C_2 from Fig. 2 appear in (25) only as a sum they can be set equal without any loss of generality. Additionally, they only appear in the expression for ε_{yy} so, it is equivalent to setting the permittivity of the two constitutive networks equal. Using (25) and $C_1 = C_2$, or $Y_{x1} + Y_{x2} + Y_{x1}Y_{x2}Z_x = Y_{z1} + Y_{z2} + Y_{z1}Y_{z2}Z_z$, the equivalent material parameters in terms of the circuit elements are,

$$\omega \mu_{xx} d = -2j Z_z, \qquad \omega \mu_{zz} d = -2j Z_x$$

$$\omega \varepsilon_{yy} d = -4j (Y_{x1} + Y_{x2} + Y_{x1} Y_{x2} Z_x),$$

$$\omega a_{xy} d = Z_z (Y_{z1} - Y_{z2}), \quad \omega a_{zy} d = Z_x (Y_{x2} - Y_{x1}) \quad (35)$$

Generally this unit cell produces a dispersive omega medium. However, by choosing the magneto-electric coupling to satisfy $|a_{xy}| \ll \sqrt{\mu_{xx}\varepsilon_{yy}}$ and $|a_{zy}| \ll \sqrt{\mu_{zz}\varepsilon_{yy}}$, the π -networks are low-pass circuits, thereby reducing the effects of dispersion below the cutoff frequency of the π -network: $\omega_c = 2/\sqrt{L_k(C_{k1}+C_{k2})}$; where, $Z=j\omega L_k$ and $Y_1=j\omega C_{k1}$ and $Y_2=j\omega C_{k2}$ in Fig. 4 (a). Let's consider a medium with the following material parameters at 10 GHz: $\varepsilon_{yy}=2\varepsilon_0$, $\mu_{xx}=5\mu_0,\ \mu_{zz}=7\mu_0,\ a_{xy}=-a_{yx}=j0.1\sqrt{\mu_0\varepsilon_0}$, and $a_{zy}=-a_{yz}=-j0.2\sqrt{\mu_0\varepsilon_0}$. To satisfy the homogeneous limit assumption, the maximum phase delay for on axis propagation is $k_{Bx}d=\pi/5$ rad at $f_0=10$ GHz (d=0.8 mm). Using (35) the lumped elements of the unit cell in Fig.

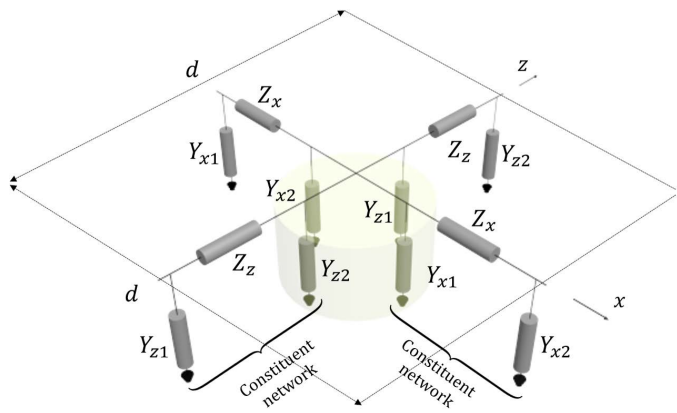


Fig. 5. A representation of the 2-D lumped element unit cell representing a 2-D omega medium composed of 1-D asymmetric π -networks comprising each constituent network.

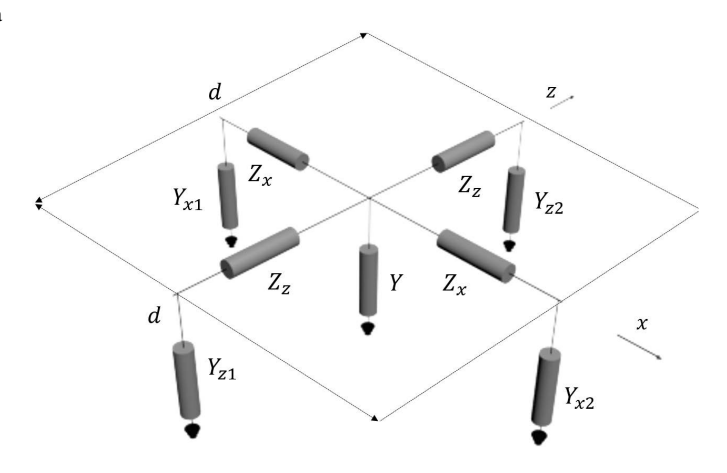


Fig. 6. A representation of the 2-D unit cell used to implement a 2-D omega medium composed of 1-D asymmetric π -networks in each constituent network. It is constructed by combining the central elements in Fig. 5, $Y = Y_{x1} + Y_{x2} + Y_{z1} + Y_{z2}$.

5 are,

$$Z_x = j\omega_0 L_x = j222\Omega, \quad Z_z = j\omega_0 L_z = j159\Omega$$

 $Y_{x1} = j\omega_0 C_{x1} = j36.6\mu\text{S}, \quad Y_{x2} = j\omega_0 C_{x2} = j188\mu\text{S}$
 $Y_{z1} = j\omega_0 C_{z1} = j59.3\mu\text{S}, \quad Y_{z2} = j\omega_0 C_{z2} = j166\mu\text{S}$ (36)

where $\omega_0 = 2\pi f_0$. These impedances and admittances are implemented with the inductors and capacitors in Table I. Substituting (36) into (35) yields the following effective material parameters,

$$\mu_{xx} = 2\frac{L_z}{d} = 5.03\mu_0, \quad \mu_{zz} = 2\frac{L_x}{d} = 7.02\mu_0,$$

$$\varepsilon_{yy} = \frac{4}{d}(C_{x1} + C_{x2} - \omega^2 C_{x1} C_{x2} L_x) = (2.02 - 0.014(\frac{\omega}{\omega_0})^2)\varepsilon_0,$$

$$a_{xy} = -\omega \frac{L_z(C_{z1} - C_{z2})}{d} = 0.1\frac{\omega}{\omega_0} \sqrt{\mu_0 \varepsilon_0},$$

$$a_{zy} = -\omega \frac{L_x(C_{x2} - C_{x1})}{d} = -0.2\frac{\omega}{\omega_0} \sqrt{\mu_0 \varepsilon_0} \quad (37)$$

Considering the form of the material parameters in (37), the permeability is non-dispersive and the permittivity does not

exhibit significant dispersion if,

$$\omega \ll \min\left(\frac{1}{\sqrt{L_x(C_{x1} + C_{x2})}}, \frac{1}{\sqrt{L_z(C_{z1} + C_{z2})}}\right)$$
 (38)

due to the low-pass nature of the design. However, the magneto-electric terms exhibit a linear frequency dispersion: $a_{xy} \propto \omega$ and $a_{zy} \propto \omega$. Therefore, even at low frequencies there will be appreciable frequency variation in the magneto-electric terms.

The equivalent material parameters for the unit cell with circuit elements given in Table I are plotted in Fig. 7 over a frequency range from 0 to 15 GHz. The permittivity and permeability show no dispersion over this frequency range, but there is dispersion in the magneto-electric terms, as expected. Due to the relatively small magnitude of the magneto-electric terms, compared to $\sqrt{\mu_{xx}\varepsilon_{yy}}$ and $\sqrt{\mu_{zz}\varepsilon_{yy}}$, the dispersion curves will not diverge significantly from the desired omega materials response below 10 GHz. However, dispersion in the magneto-electric term has significant effects on the imaginary part of the wave impedance. At 9 GHz it has been reduced to 90% of its value at 10 GHz. This will ultimately place bandwidth limitations on devices designed with these structures.

Using Keysight's Advanced Design System (ADS), isofrequency contours were computed for the unit cell at 8, 9, and 10 GHz. The dispersion of the unit cell was characterized by terminating its ports in the appropriate Bloch impedances given by (20) and (21). The input terminals were driven in the x and z-directions with voltage sources V_x and V_z such that a plane wave was established in the periodic network. The necessary relationship between the voltage sources to produce a plane wave with a given wave vector $k_B = k_{Bx}\hat{x} + k_{Bz}\hat{z}$ in the periodic network is provided in [8]. The simulation was performed by setting V_x to 1V and the input terminal in the z-direction was driven with [8],

$$V_z(k_{Bx}d) = \frac{A_1 + D_1}{A_2 + D_2} \frac{\cos(k_{Bz}d/2)}{\cos(k_{Bx}d/2)} e^{j\frac{k_{Bz} - k_{Bx}}{2}d}$$
(39)

The voltage excitation's were defined to provide a desired $k_{Bx}d$ and the resulting $k_{Bz}d$ was retrieved from the simulation. This was done using the full dispersion relationship for the network, (19), and expressing $k_{Bz}d$ in terms of the network parameters and $k_{Bx}d$. Therefore, (39) can be expressed solely in terms of the network parameters and $k_{Bx}d$. To obtain the isofrequency contours $k_{Bx}d$ was swept from $-\pi/5$ to $\pi/5$ rad while measuring $k_{Bz}d$ across the unit cell. The results are shown in Fig. 8. There is close agreement between the simulated isofrequency contours and the analogous omega medium's isofrequency contours. Thus, indicating that the propagation characteristics match that of the omega medium within this frequency range.

B. Omega Layers for Impedance Matching

In [25], a 1-D propagation model was used to impedance match a normally incident plane wave with a Huygens' bianisotropic metasurface separating two regions of dielectric. Further, it was shown that an omega-type response could be used to control the normal phase delay. In this section,

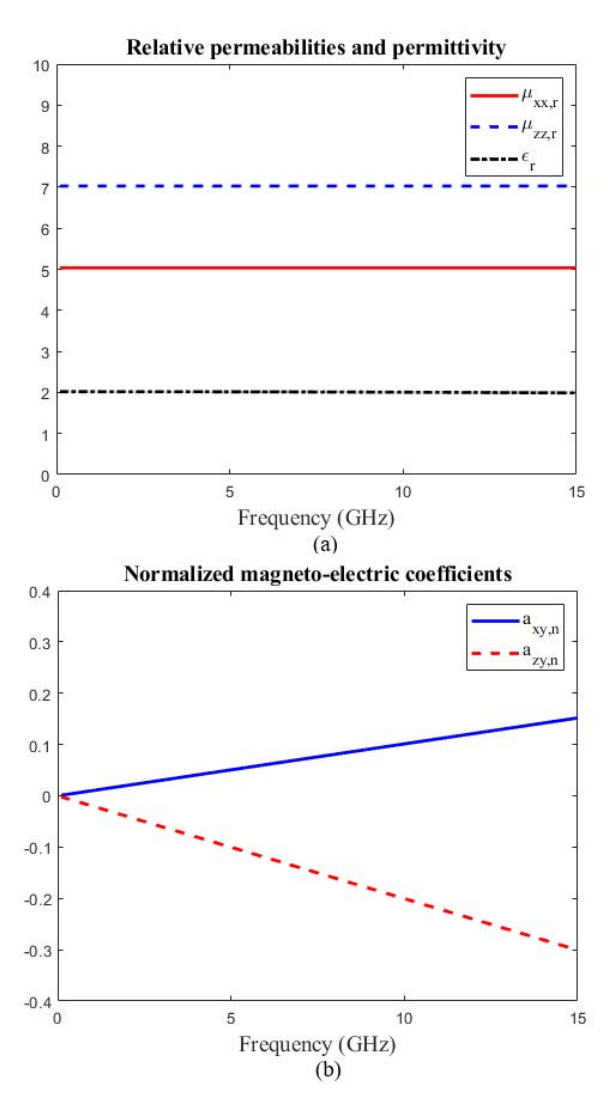


Fig. 7. Material parameters of the unit cell shown in Fig. 6, composed of the elements given in Table I up to 15 GHz. (a) Relative permittivity and permeabilities (b) Normalized magneto-electric coefficients, $a_{yz}/\sqrt{\mu_0\varepsilon_0}$ and $a_{yx}/\sqrt{\mu_0\varepsilon_0}$.

a 2-D circuit-based omega medium will be used to design an impedance matching layer that provides a desired normal phase delay but also translates the incident power density profile of a wavefront. The impedance matching condition and desired transmission phase are controlled with the tangential polarizabilities in the layer and the direction of power flow is controlled by the normal polarizabilites.

To demonstrate this functionality, the circuit simulator ADS is used to simulate two isotropic half spaces of different materials separated by an omega medium slab with thickness d. The slab is infinite in the x-y plane and has finite extent in the z-direction. Therefore, \hat{z} is normal to the slab while \hat{x} and \hat{y} are tangential to the surface of the slab. The simulation domain consists of three regions: medium 1, the omega slab, and medium 2. The two isotropic regions (medium 1 and 2) are implemented using the isotropic lumped element unit cells shown in Fig. 9, and the unit cell shown in Fig. 6 was used to realize the omega slab. At the edges of the domain, each region

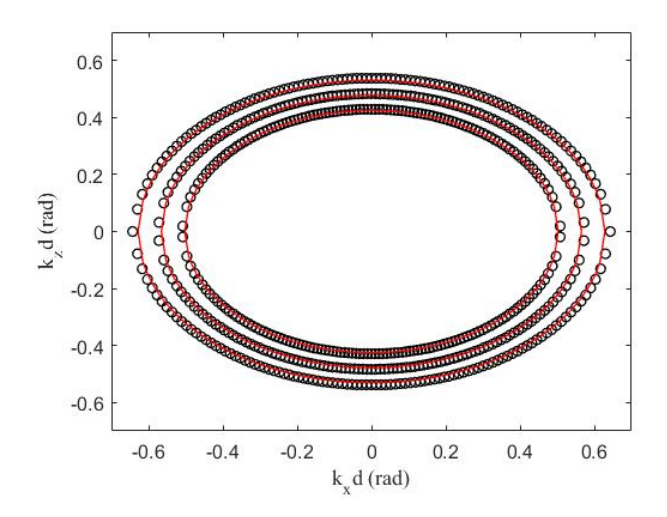


Fig. 8. Isofrequency contours at 8 GHz (inner), 9 GHz (middle), and 10 GHz (outer) for the unit cell shown in Fig. 6 with elements given in Table I. The black circles are the dispersion characteristics extracted from an ADS simulation of the unit cell. The red solid lines are calculated using (16) for the equivalent omega medium.

is terminated in appropriate Bloch impedances to emulate an unbounded medium, as shown in Fig. 10.

To design the slab, an omega medium separating two dielectrics illuminated by a TE wave propagating in the xz plane is analyzed. The slab is designed to impedance match the two regions, provide a transmission phase, ϕ_d , in the \hat{z} (normal) direction and support a prescribed angle of power flow, θ_S . A plane wave is incident from the first medium at an angle, θ_i (relative to the z-axis). The angle of incidence sets the normal wave impedance in medium 1, η_{z1} . Phasematching sets the tangential wavenumber in the slab, as well as in medium 2. This determines the normal wave impedance in medium 2, η_{z2} . The phase delay ϕ_d determines the necessary normal wavenumber, k_z . The normal wave impedance, η_z , in the omega medium is determined by η_{z1} and η_{z2} . The design equations are calculated using 1-D transmission-line analysis (see Fig. 11). By setting the input impedance of the transmission line equal to the incident wave impedance, $Z_{\rm in} = \eta_1$, and specifying the normal phase delay, ϕ_d , across the transmission line, a system of equations can be written. If $\phi_d \neq n\pi$ for $n \in \mathbb{Z}$ then the system of equations can be solved for the wavenumber and wave impedance of the omega medium as follows,

$$\tan k_z d = \frac{\sqrt{4\eta_{z1}\eta_{z2}\tan^2\phi_d - (\eta_{z2} - \eta_{z1})^2}}{\eta_{z1} + \eta_{z2}}$$
(40)

$$\eta_z' = \frac{\sqrt{4\eta_{z1}\eta_{z2}\tan^2\phi_d - (\eta_{z2} - \eta_{z1})^2}}{2\tan\phi_d}$$
(41)

$$\eta_z^{\prime\prime} = \frac{\eta_{z2} - \eta_{z1}}{2\tan\phi_d} \tag{42}$$

There exist real solutions to (40) and (41) if the following inequality is satisfied,

$$|\cos \phi_d| \le \frac{\sqrt{\eta_{z1}\eta_{z2}}}{(\eta_{z1} + \eta_{z2})/2}$$
 (43)

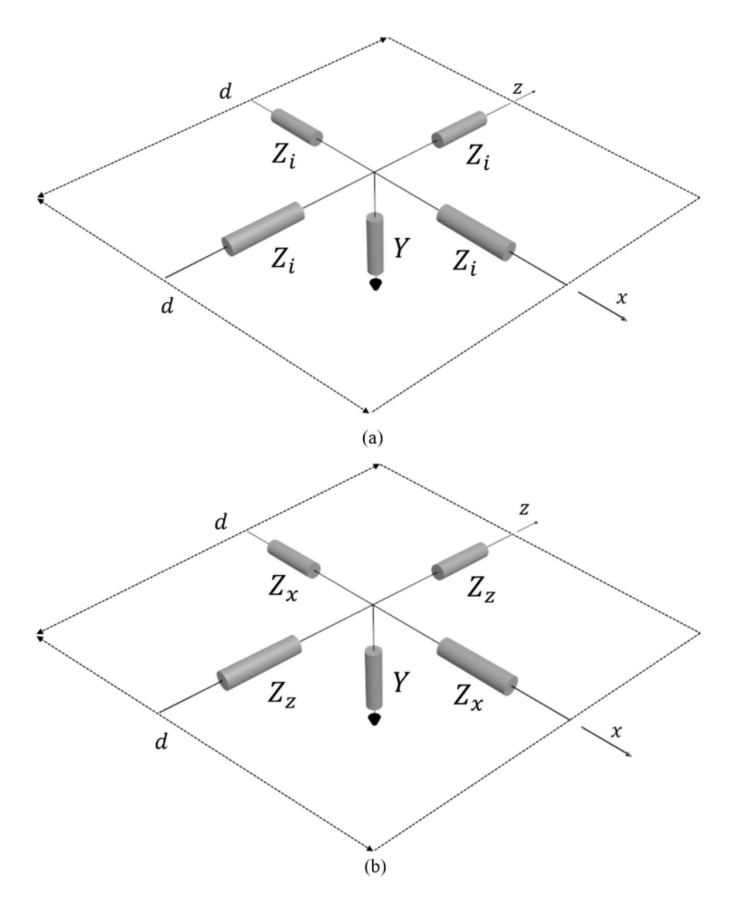


Fig. 9. (a) Lumped element unit cell used to implement a 2-D isotropic medium, consisting of two identical symmetric branches along the principal axes (x and z directions). (b) Lumped element unit cell used to implement anisotropic medium, consisting of two different symmetric branches along the principal axes.

The time-averaged Poynting vector for a TE plane wave propagating in a lossless, reciprocal omega medium in the x-z plane is given by,

$$\overline{S} = \frac{1}{2} \overline{E} \times \overline{H}^* = \frac{E_y}{2} (H_z^* \hat{x} - H_x^* \hat{z})
= \frac{|E_y|^2}{2} (\frac{\eta_x}{|\eta_x|^2} \hat{x} + \frac{\eta_z}{|\eta_z|^2} \hat{z}) = S_x \hat{x} + S_z \hat{z} \quad (44)$$

The angle of power flow, θ_S , is defined as the angle that the time-averaged Poynting vector makes with the z-axis. This angle θ_S can be expressed in terms of the wave impedances along the principal axes as follows,

$$\tan \theta_S = \frac{\Re(S_x)}{\Re(S_z)} = \frac{\eta_x'}{\eta_z'} \left(\frac{{\eta_z'}^2 + {\eta_z''}^2}{{\eta_z'}^2 + {\eta_z''}^2} \right) \tag{45}$$

where $\eta_i = \eta_i' + j\eta_i''$ for i = x, z. From (45), it is clear that controlling power flow in the omega medium and impedance matching in the x and z-directions is not possible. Specifying the direction of power flow and impedance matching in the normal direction leaves only one degree of freedom in (45). As a result either the real or the imaginary part of the transverse wave impedance, η_x can be matched, while the

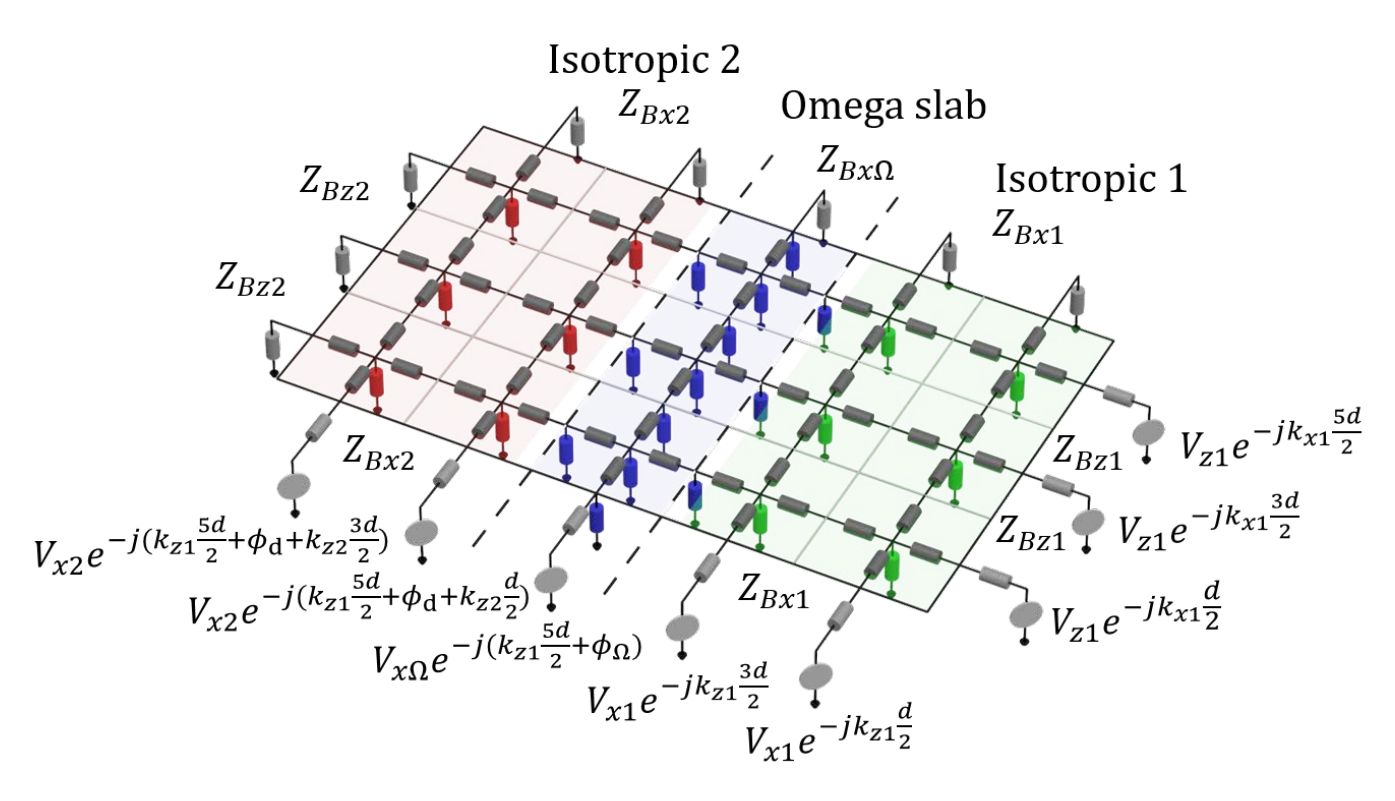


Fig. 10. A circuit network representation of two different isotropic half spaces separated by a slab of omega medium. The slab acts as a matching layer which provides a desired phased delay ϕ_d in the z-direction. The omega impedance matching layer is shown in the middle between the two isotropic grids. The boundary of the domain is terminated in the appropriate Bloch impedances to emulate an unbounded structure. The excitation is set by the voltage sources on the boundary. In medium 1 and 2, the amplitudes $(V_{x1}$ and $V_{x2})$ and phases of the voltage sources are set by the desired incident and transmitted fields. The source connected to the slab provides the amplitude $(V_{x\Omega})$ and phase necessary to emulate the standing wave that exists in the infinite slab.

other is determined by (45). Solving (16)–(18) for the material parameters in terms of k_x , k_z , η_x' , η_x'' , η_x'' , η_z' and η_z'' yields,

$$\varepsilon_{yy} = \frac{1}{\omega} \left(\frac{k_z}{\eta_z'} + \frac{k_x}{\eta_x'} \right)$$

$$\mu_{xx} = \frac{k_z}{\omega} \frac{{\eta_z'}^2 + {\eta_z''}^2}{{\eta_z'}}, \quad \mu_{zz} = \frac{k_x}{\omega} \frac{{\eta_x'}^2 + {\eta_x''}^2}{{\eta_x'}}$$

$$a_{xy} = \frac{k_z}{\omega} \frac{{\eta_z'}}{{\eta_z'}}, \quad a_{zy} = -\frac{k_x}{\omega} \frac{{\eta_x'}}{{\eta_x'}}$$
(46)

Therefore, an impedance matching omega slab that provides a desired phase delay and power flow direction can be designed in the following manner. First, phase-matching is applied at the two boundaries of the slab then (40)–(42) and (45) are solved for the necessary normal wavenumber and wave impedances in the slab. Next, (46) is used to determine the necessary omega material parameters as a function of either the real or imaginary part of the transverse wave impedance. While the other component is given by (45).

As an example, an impedance matching omega slab is designed for a TE plane wave propagating from medium 1 into medium 2. The wave is incident on the slab separating the two regions of non-magnetic dielectrics. Medium 1 has $\varepsilon_r=10$ and medium 2 is free space. The angle of incidence is $\theta_i=10^\circ$. The normal wave impedance in media 1 and 2 are $\eta_{z1}=121\Omega$ and $\eta_{z2}=451\Omega$, respectively. To limit spatial dispersion in all three regions, the unit cell dimension is chosen to be $d=\frac{\lambda_0}{10\sqrt{10}}=0.95 \mathrm{mm}$ at 10 GHz. This results

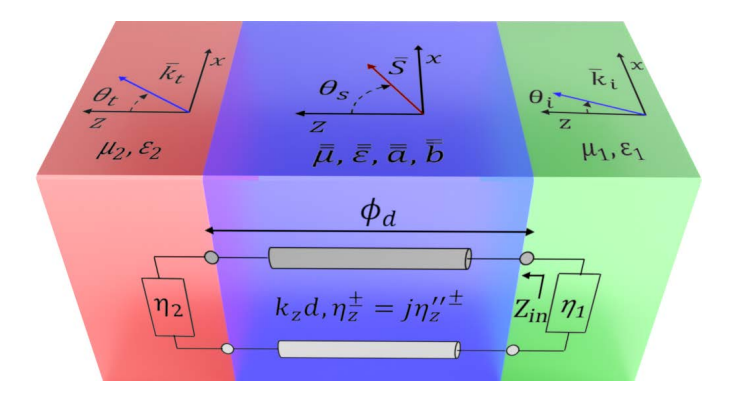


Fig. 11. Front face: Transmission-line analogy for analyzing propagation through a slab separating two half spaces characterized by their wave impedances η_1 and η_2 . Top face: Definition of the angles θ_i , θ_S , and θ_t in the corresponding regions: medium 1 (right), omega slab (center), or medium 2 (left).

in the following lumped elements for the two isotropic grids (see Fig. 9),

$$Z_{i1} = j37.4\Omega$$
, $Y_{i1} = j5.3 \text{mS}$ (a)
 $Z_{i2} = j37.4\Omega$, $Y_{i2} = j0.53 \text{mS}$ (b)
$$(47)$$

where Z_{i1} and Y_{i1} refer to medium 1 and Z_{i2} and Y_{i2} to medium 2. In the design of the impedance matching slab the

imaginary part of the tangential wave impedance, η_x'' , is a free variable and is chosen to be zero. In this case the real part of the transverse wave impedance, or equivalently μ_{zz} , is used to control the direction of power flow. In this example, the direction of the Poynting vector is selected to demonstrate extreme redirection of power to an unbound propagating wave in the second medium. Using the design procedure outlined earlier in this section, the slab is designed to provide a normal phase delay of $\phi_d=36^\circ$ and support a Poynting vector at $\theta_S=89.5^\circ$ relative to the z-axis. These conditions result in the following material parameters for the slab: $\varepsilon_{yy}=28.6\varepsilon_0$, $\mu_{xx}=1.8\mu_0$, $\mu_{zz}=0.013\mu_0$, $a_{xy}=-a_{yx}=-2.9\sqrt{\mu_0\varepsilon_0}$, and $a_{zy}=-a_{yz}=0$. From (35), the necessary lumped impedances and admittances to implement the slab, using Fig. 6, are calculated,

$$Z_x = j0.48\Omega$$
, $Z_z = j67.4\Omega$, $Y_{x1} = j1.89$ mS,
 $Y_{x2} = j1.89$ mS, $Y_{z1} = -j2.95$ mS, $Y_{z2} = j5.61$ mS (48)

For comparison, an anisotropic slab with the same power flow angle and phase delay is designed. The necessary normal wavenumber, k_z , and wave impedance, η_z , for the anisotropic slab is also determined using 1-D transmission-line analysis, as shown in Fig. 11 with $\eta_z''=0$. Solving for the normal wavenumber in terms of the normal phase delay yields,

$$\tan k_z d = \frac{\eta_{z2}}{\eta_z} \tan \phi_d \tag{49}$$

In order to minimize reflections, the normal wave impedance of the slab is optimized since impedance matching with an arbitrary phase delay is not possible with an anisotropic medium. The normal wave impedance is optimized by solving for the magnitude of the reflection coefficient as a function of the normal wave impedance in the anisotropic medium, $|\Gamma(\eta_z)|$. By applying the first and second derivative tests to $|\Gamma(\eta_z)|$, the wave impedance is found in terms of the normal phase delay, impedance of the incident wave (η_{z1}) , and load impedance (η_{z2}) . This procedure yields the following optimal wave impedance,

$$\eta_z = \frac{|\sin \phi_d| \eta_{z2}}{\sqrt{(\cos^2 \phi_d + (\frac{\eta_{z2}}{\eta_{z1}})^2 \sin^2 \phi_d)^{1/2} - \cos^2 \phi_d}}$$
 (50)

Using the optimal normal wave impedance, η_z , for the anisotropic medium, and the wavenumber from (49), the following material properties are calculated for the anisotropic medium: $\varepsilon_{yy}=125.3\varepsilon_0$, $\mu_{xx}=2.8\mu_0$, $\mu_{zz}=0.0026\mu_0$. The anisotropic slab was implemented using the lumped element unit cell shown in Fig. 9 with the following lumped elements,

$$Z_x = j97.3 \text{m}\Omega, \quad Z_z = j104.8\Omega, \quad Y = j66.1 \text{mS}$$
 (51)

The anisotropic and omega slabs were simulated in Keysight's ADS using a grid similar to Fig. 10. The results are shown in Fig. 12 and 13, for a domain where each isotropic region is 25x51 unit cells and the slabs are 1x51 unit cells. In both cases there is a phase delay of 36° . Since the optimal wave impedance for the anisotropic slab results in a reflectance of $|\Gamma|^2 = 0.13$, there are appreciable reflections present in Fig. 12. However, there are no reflections for the omega slab, as

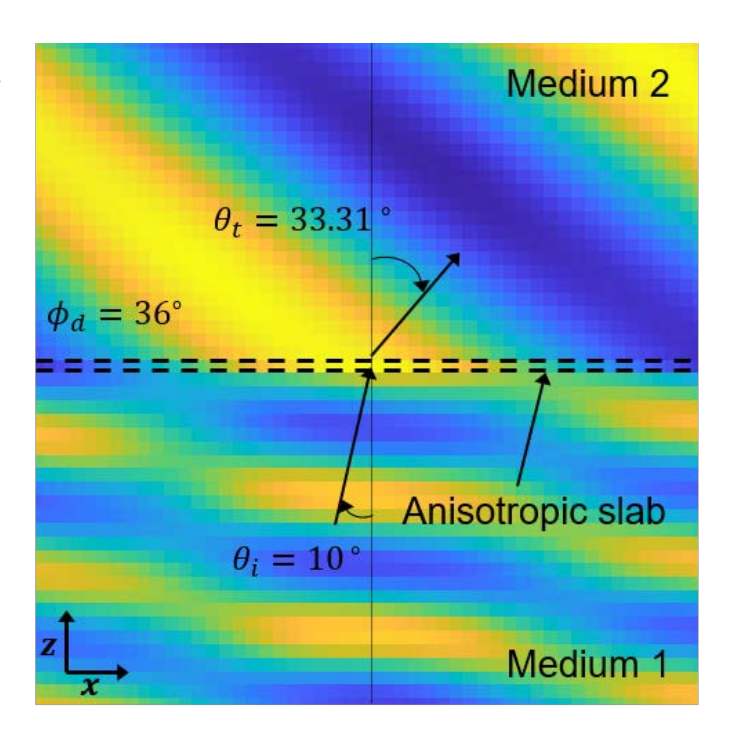


Fig. 12. Simulation results using Keysight's ADS for the instantaneous voltage (electric field) when a TE wave is incident at $\theta_i=10^\circ$ on an anisotropic slab. The slab is designed to provide a phase delay $\phi_d=36^\circ$ in the z-direction and supports a Poynting vector directed at $\theta_S=89.5^\circ$. The anistropic medium provides the appropriate phase delay, but suffers from significant reflections even for an optimized impedance value. The three regions are implemented using the lumped element unit cells in Fig. 9.

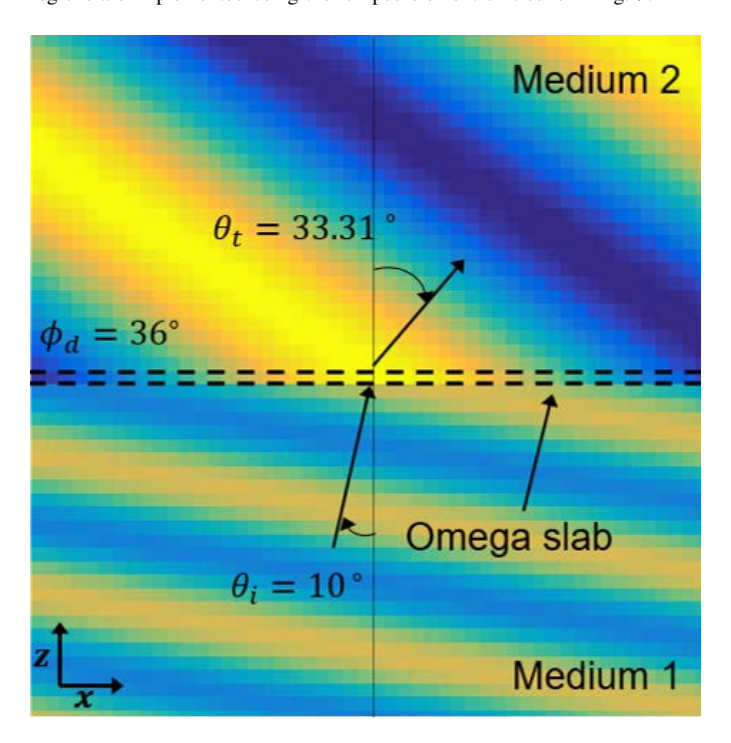


Fig. 13. Simulation results using Keysight's ADS for the instantaneous voltage (electric field) when a TE wave is incident at $\theta_i=10^\circ$ on an omega slab that provides a phase delay $\phi_d=36^\circ$ in the z-direction and supports a Poynting vector directed at $\theta_S=89.5^\circ$. In contrast to the anisotropic slab, the omega slab provides the desired phase delay in a reflectionless manner. The three regions are implemented using a lumped element grid similar to Fig. 10.

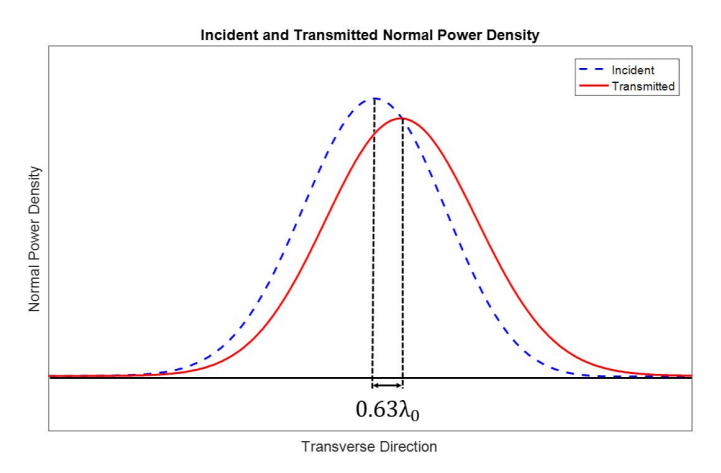


Fig. 14. Simulation results from Keysight's ADS for the incident and transmitted normal power density profiles along the boundaries of the omega matching layer with a Gaussian illumination, $w_0=5.4\lambda_0$. The incident power density (dashed line) profile is shifted in the transverse direction. The lateral shift of the peak in transmitted power density (solid line) profile corresponds to a lateral displacement of $0.63\lambda_0$ over a distance of $0.03\lambda_0$. Note that the total power across the slab is conserved. The broadening of the transmitted profile accounts for the observed decrease in peak amplitude, so it is lossless and reflectionless as expected.

shown in Fig. 13.

To verify the direction of power flow within the omega slab, the slab was illuminated by a Gaussian beam with a beam waist, $w_0 = 5.4\lambda_0$. The incident and transmitted power densities across the slab were simulated in Keysight's ADS for a 3x601 unit cell grid, similar to Fig. 10, where all three regions are composed of 1x601 unit cell grids. In Fig. 14, it is observed that the beam is laterally shifted by $0.63\lambda_0$ over a distance of approximately $0.03\lambda_0$. This lateral shift does not correspond to an angle of 89.5°. This is due to the presence of forward and reverse traveling waves in the impedance matching omega slab, resulting in a different net power flow angle. The theoretical net power flow angle across the slab is calculated by determining the total fields in the slab and finding the average transverse and normal power densities to calculate the average Poynting vector. This procedure results in a theoretical average power flow angle of 87.9° if $\theta_S = 89.5^{\circ}$ in the slab. The simulated direction of power flow was found to be 87.3°, which is in close agreement with the theoretical value. The 0.6° difference is likely due to the fact that the Gaussian beam is not a plane wave and the theoretical value assumes a plane wave illumination.

V. CONCLUSION

A circuit-based approach to synthesizing and simulating 2-D omega materials was presented. A 2-D periodic circuit network, composed of four 1-D asymmetric transmission (ABCD) matrices (constituent networks) was analyzed. Then an equivalency between the periodic circuit network and an omega medium was established in the homogeneous limit. For validation, the propagation characteristics of a lumped element unit cell emulating an omega medium was simulated in the commercial circuit solver Keysight ADS. These results were in close agreement with those of the analogous omega medium. Additionally, a 2-D omega medium was used to design an

impedance matching layer that utilizes normal polarizabilities to control power flow. The impedance matching layer provides a desired normal phase delay and laterally translates an incident beam's power density profile. The impedance matching layer illustrates the extreme control over phase and power that 2-D omega media offer while remaining electrically small. This capability makes them a promising candidate to reduce the size of beamforming networks.

This work has focused on modeling and realizing 2-D omega media with circuit networks. Practical structures with 2-D omega responses are necessary to realize microwave devices. Practical structures with these material responses could be realized as printed circuit structures, additively manufactured structures composed of omega-particles, [38], or a media composed of loaded loops and dipoles similar to [39]. Here polarization conserving media were considered however, the circuit network model could include more general material responses by extending Kron's work, [40], to include bianisotropic media. This could be accomplished by developing a dual network for transverse magnetic (TM) propagation in an analogous manner to this work. By coupling the network presented in this work to the dual network, polarization conversion could be achieved allowing for the design of devices with phase, amplitude and polarization control.

ACKNOWLEDGMENT

This work was supported by the National Science Foundation, under GOALI grant 1807940. The authors would like to acknowledge helpful and stimulating discussions with Dr. Gurkan Gok from United Technologies Research Center.

REFERENCES

- G. A. Campbell, "XXX. On loaded lines in telephonic transmission," The London, Edinburgh, and Dublin Philosophical Magazine and Journal of Science, 1903, 5:27, 313–330.
- [2] G. V. Eleftheriades and K. G. Balmain, Negative Refraction Metamaterials: Fundamental Principles and Applications. Wiley-IEEE Press, New Jersey, 2005.
- [3] C. Caloz and T. Itoh, "Application of the transmission line theory of left-handed (LH) materials to the realization of a microstrip LH line," in Proc. IEEE Antennas and Propagation Society Int. Symp., San Antonio, TX, Jun. 2002, vol. 2, pp. 412–415.
- [4] V. B. Veselago, "The electrodynamics of substances with simultaneously negative values of ε and μ," Sov. Phys.-Usp., vol. 10, no.4, pp. 509–514, Jan.-Feb. 1968.
- [5] P. B. Johns and R. L. Beurle, "Numerical solution of 2-dimensional scattering problems using a transmission-line matrix," *PROC. IEE*, vol. 118, No. 9, pp. 1203-1208, Sept. 1971.
- [6] A. Grbic and G. V. Eleftheriades, "A backward-wave antenna based on negative refractive index L-C networks," in Proc. IEEE Antennas and Propagation Int. Symp., San Antonio, TX, Jun. 2002, vol. 4, pp. 340— 343.
- [7] A. Grbic and G. V. Eleftheriades, "Experimental verification of backward-wave radiation from a negative refractive index metamaterial," *Journal of Applied Physics*, 92, 5930 (2002)
- [8] A. Grbic and G.V. Eleftheriades, "Periodic Analysis of a 2-D Negative Refractive Index Transmission Line Structure," *IEEE Trans. Antennas Propag.*, vol. 51, pp. 2604–2611, Oct. 2003.
- [9] A. Grbic, Super Resolving Negative-Refractive-Index Transmission-Line Lenses. PhD thesis, The Edward S. Rogers Sr. Department of Electrical and Computer Engineering, University of Toronto, 2005. pp 54–60.
- [10] C. Caloz, C.H. Ahn, and T. Itoh, "Analysis 2D finite-size metamaterials by the transmission matrix method," in Proc. IEEE Antennas and Propagation Society Int. Symp., Washington, DC, Jul. 2005, vol. 38, pp. 2—5.

- [11] A. Sanada, C. Caloz, and T. Itoh, "Characteristics of the composite right/left-handed transmission lines," *IEEE Microw. Wirel. Compon. Lett.*, vol. 14, no. 2, pp.68–70, Feb. 2004.
- [12] G. V. Eleftheriades, A. Iyer, and P. Kremer, "Planar Negative Refractive Index Media Using Periodically L-C Loaded Transmission Lines," *IEEE Trans. Microw. Theory Tech.*, vol. 50, pp. 2702–2712, Dec. 2002.
- [13] A. Grbic and G. V. Eleftheriades, "Overcoming the Diffraction Limit with a Planar Left-Handed Transmission-Line Lens," *Phys. Rev. Lett.*, vol. 92, no. 11, p. 117403, 2004.
- [14] K. G. Balmain, A. A. E. Luttgen, and P. C. Kremer, "Power flow for resonance cone phenomena in planar anisotropic metamaterials," *IEEE Trans. Antennas Propag.*, vol. 51, no. 10, pp. 2612—2618, Oct. 2003.
- [15] J. B. Pendry, D. Schurig, and D. R. Smith, "Controlling electromagnetic fields," *Science*, vol. 312, pp. 1780–1782, Jun. 2006.
- [16] U. Leonhardt, "Optical conformal mapping," Science, vol. 312, no. 5781, pp. 1777–1780, Jun. 2006.
- [17] G. Gok and A. Grbic, "Tensor Transmission-Line Metamaterials," *IEEE Trans. Antennas Propag.*, vol. 58, pp. 1559–1566, May 2010.
- [18] D.-H. Kwon and CD Emiroglu, "Non-Orthogonal Grids in Two-Dimensional Transmission-Line Metamaterials," *IEEE Trans. Antennas Propag.*, vol. 60, pp. 4210–4218, Sept. 2012.
- [19] M. Zedler and GV Eleftheriades, "Anisotropic Transmission-Line Metamaterials for 2-D Transformation Optics Applications," *Proceedings of the IEEE*, vol. 99 No. 10, pp. 1634–1645, Oct. 2011.
- [20] J. Vehmas, S. Hrabar, and S. Tretyakov, "Omega transmission lines with applications to effective medium models of metamaterials," *Journal of Applied Physics*, 115, 134905 (2014)
- [21] C. Pfeiffer and A. Grbic, "Bianisotropic Metasurfaces for Optimal Polarization Control: Analysis and Synthesis," *Phys. Rev. Appl.*, 2, 044011 (2014).
- [22] A. Epstein and G.V. Eleftheriades, "Arbitrary Power-Conserving Field Transformations With Passive Lossless Omega-Type Bianisotropic Metasurfaces," *IEEE Trans. Antennas Propag.*, vol. 64, pp. 3880–3894, Sept. 2016.
- [23] V.S. Asadachy et al., "Perfect control of reflection and refraction using spatially dispersive metasurfaces," *Phys. Rev. B*, 94, 075142 (2016).
- [24] J.P.S Wong, A. Epstein, and G.V. Eleftheriades, "Reflectionless Wide-Angle Refracting Metasurfaces," *IEEE Antennas Wirel Propag. Lett.*, 15, 1293(2016).
- [25] A. H. Dorrah, M. Chen and G.V. Eleftheriades, "Bianisotropic Huygens' Metasurface for Wideband Impedance Matching Between Two Dielectric Media," *IEEE Trans. Antennas Propag.*, vol. 66, no. 9, Sept. 2018.
- [26] B. O. Raeker and A. Grbic, "Paired Metasurfaces for Amplitude and Phase Control of Wave Fronts," in Proc. IEEE Antennas and Propagation Int. Symp., Boston, MA, July 2018, pp. 1479–1480.
- [27] B. O. Raeker and A. Grbic, "Compound Metaoptics for Amplitude and Phase Control of Wave Fronts," *Phys. Rev. Lett.* 122, 113901(2019).
- [28] A. H. Dorrah and G.V. Eleftheriades, "Bianisotropic Huygens' Metasurface Pairs for Nonlocal Power-Conserving Wave Transformations," *IEEE Antennas Wirel. Propag. Lett.*, vol. 17, no. 10, Oct. 2018.
- [29] S.N. Tcvetkova et al., "Near-perfect conversion of a propagating plane wave into a surface wave using metasurfaces," Phys. Rev. B, 97, 115447
- [30] V. Popov et al., "Omega-bianisotropic metasurface for converting a propagating wave into a surface wave," Phys. Rev., 100, 125103 (2019).
- [31] M. Chen et al., "Theory, design, and experimental verification of a reflectionless bianisotropic Huygens' metasurface for wide-angle refraction," *Phys. Rev. B*, 97, 125433 (2018).
- [32] M. Albooyeh et al., "Equivalent realizations of reciprocal metasurfaces: Role of tangential and normal polarization," *Phys. Rev. B* 95, 115435 (2017).
- [33] G. Gok and A. Grbic, "Tailoring the phase and power flow of electromagnetic fields," *Phys. Rev. Lett.* 111, 233904(2013).
- [34] A. Alu, "First-principles homogenization theory for periodic metamaterials," *Phys. Rev. B* 84, 075153 (2011).
- [35] A. Shaltout, V. Shalaev, and A. Kildishev, "Homogenization of bianistropic metasurfaces," *Optics Express*, vol. 21, no. 19, p. 21941, Nov. 2013
- [36] M. M. I. Saadoun and N. Engheta, "A Reciprocal Phase Shifter Using Novel Pseudochiral or Ω Medium," *Microwave Opt. Tech- nol. Lett.*, Vol. 5, 1992, pp. 184–188.
- [37] D.M. Pozar, Microwave Engineering, 4th ed. New York: Wiley, 2011 pp. 381–385.
- [38] A. Serdyukov, I. Semchenko, S. Tretyakov and A Sihvola, *Electromagnetics of Bi-anisotropic Materials Theory and Applications*. Gordon and Breach Science Publishers, Singapore 2001.

- [39] S. Rudolph and A. Grbic, "A Broadband Three-Dimensionally Isotropic Negative-Refractive-Index Medium," *IEEE Trans. Antennas Propag.*, vol. 60, no. 8, Aug. 2012.
- [40] G. Kron, "Equivalent Circuit of the Field Equations of Maxwell-I," Proc. IRE, vol. 32, no. 5, Nov. 1944.



Luke Szymanski (F'15) received the B. Sc. in Electrical Engineering (Summa Cum Laude) from the University of Texas at Dallas in 2015. In 2016, he joined Professor Grbic's group at the University of Michigan as a Ph.D. student. His research interests include analytical electromagnetics, bianisotropic materials, and inverse-design methods.



Anthony Grbic (S'00 - M'06 - SM'14 - F'16) received the B.A.Sc., M.A.Sc., and Ph.D. degrees in electrical engineering from the University of Toronto, Toronto, ON, Canada, in 1998, 2000, and 2005, respectively. In January 2006, he joined the Department of Electrical Engineering and Computer Science, University of Michigan, Ann Arbor, MI, USA, where he is currently a Professor. His research interests include engineered electromagnetic structures (metamaterials, metasurfaces, electromagnetic band-gap materials, frequency-selective surfaces),

plasmonics, antennas, microwave circuits, wireless power transmission, and analytical electromagnetics/optics. Dr. Grbic served as Technical Program Co-Chair in 2012 and Topic CoChair in 2016 and 2017 for the IEEE International Symposium on Antennas and Propagation and USNC-URSI National Radio Science Meeting. He was an Associate Editor for IEEE Antennas and Wireless Propagation Letters from 2010 to 2015. He is currently the Vice Chair of AP-S Technical Activities, Trident Chapter, IEEE Southeastern Michigan Section. Dr. Grbic was the recipient of AFOSR Young Investigator Award as well as NSF Faculty Early Career Development Award in 2008, the Presidential Early Career Award for Scientists and Engineers in January 2010. He also received an Outstanding Young Engineer Award from the IEEE Microwave Theory and Techniques Society, a Henry Russel Award from the University of Michigan, and a Booker Fellowship from the United States National Committee of the International Union of Radio Science in 2011. He was the inaugural recipient of the Ernest and Bettine Kuh Distinguished Faculty Scholar Award in the Department of Electrical and Computer Science, University of Michigan in 2012.